N doping of TiO$_2$ nanocrystal for efficient photodegradation of organic pollutants under ultraviolet and visible light irradiation

Xiaoyou YU^1 , Qianrui LV^2, *
^{1}Beijing Energy Technology Co. Ltd., Beijing, China
^{2}School of Science, Beijing Jiaotong University, Beijing, China

Abstract: To decrease the band gap of TiO$_2$ and enhance its photocatalytic performance, in this work, N-doped nanocrystalline TiO$_2$ is synthesized successfully through a simple sol-gel synthesis process with dicyandiamide used as N source. The N-doped TiO$_2$ photocatalysts have been characterized in detail by means of powder X-ray diffraction, Raman spectroscopy, infrared spectroscopy, UV-vis spectroscopy, X-ray photoelectron spectroscopy, and scanning electron microscope. The photocatalytic activities of N-doped TiO$_2$ to different organic pollutants are significantly different. Using 2×10^{-5} mol/L methylene blue as the target pollutant, N-doped TiO$_2$ can produced approximately 100% conversion within 40 min, the photocatalytic degradation ability of which is equal or superior to commercial or bare TiO$_2$. The ameliorated photocatalytic activity of N-doped TiO$_2$ photocatalysts is attributed to the appropriate crystallinity, good dispersibility, modified Zeta potential, and increased absorption.

Key words: photocatalysis, nanocrystals, nitrogen doping, titanium oxide, organic pollutants

1. Introduction

Photocatalytic technology is a robust method to solve environmental pollution because of its green, safety and high efficiency. As a promising photocatalyst, TiO$_2$ possesses admirable merits such as low cost, high corrosion resistance, and nonhazardous nature. As a result, it has been widely used in the fields of pollutant treatment, hydrogen generation via photocatalytic water splitting and self-cleaning [1–5]. However, the high band gap energy (3.2 eV) of TiO$_2$ corresponds to the wavelength of ultraviolet light (<387 nm), [6] which significantly hinders the full use of solar light because it can only capture approximately 5% of total solar irradiation [6].

Atom doping is regarded as a common approach to decrease the TiO$_2$ band gap [7–15]. Especially, substituting some of the oxygen atoms by nitrogen atoms is an effective method because the resulting mixed states of substitutional N 2p and O 2p can narrow the band gap of TiO$_2$ so that electrons can be excited from the valence band to the conduction band by the irradiation of visible light [7,16]. In addition, oxygen vacancies produced by N-doping can effectively boost the photocatalytic performance of TiO$_2$ because oxygen vacancies can induce the rearrangement of the surrounding atoms, affecting the concentration of the surface hydroxyl and ameliorating the detachment and transfer of photo-generated carriers [17–23]. Previous studies have shown that the performance of N-doped TiO$_2$ is closely related to the raw materials and synthesis methods. For example, Asahi et al. claimed that nitrogen doping was helpful for the photoactivity of TiO$_2$ under visible light, without weakening the photoactivity under ultraviolet light [7]. However, N-doped TiO$_2$ prepared by other methods showed the degradation of photoactivity under ultraviolet irradiation [24–26]. Therefore, people have been exploring various doping methods for several years. At present, the common N doping methods include hydrothermal method [27–28], solvothermal method [29], high temperature calcination [30], sol-gel method [31], and so on. Among them, the hydrothermal method can make a large amount of N doping into TiO$_2$ nanoparticles; the solvothermal method can achieve the synthesis of nanoparticles with higher grain size and narrower particle size distribution; The calcination method is helpful to change the physical and chemical properties of the crystal, making it easier for the N to enter the TiO$_2$ crystal lattice. Recently, Ma et al. reported the N-doped TiO$_2$ via the vapor-thermal method, using urea as the N source [32]. It showed great enhancement in the adsorption coefficient and photocatalytic degradation ability.

Searching for novel synthesis methods of high-performance N-doped TiO$_2$ photocatalysts is still of great interest. In this work, we use dicyandiamide rather than common urea or ammonia as N source to prepare N-doped TiO$_2$ nanoparticles by

---

* Correspondence: lvqianrui@bjtu.edu.cn

sol-gel method. The method is relatively simple and a series of characterizations are used to prove the successful existence of N in TiO_2 lattice. The as-prepared N doped TiO_2 are used for the photocatalytic degradation of a series of organic pollutants under ultraviolet and visible light irradiation. It is found that the N doping not only improves photocatalytic activity for the photodegradation under ultraviolet light but also expands the absorption of TiO_2 in visible light and show good visible light photocatalytic activity. The N-doped TiO_2 shows equal or superior activity to commercial P25 or bare TiO_2 for the decontamination of methylene blue (MB). The effect of nitrogen doping amounts on the photodegradation ability and the difference in the degradation of different organic pollutants are also discussed.

2. Materials and methods

All reagents used in this research were analytically pure and used without further purification.

Glacial acetic acid was added to a beaker containing anhydrous ethanol at room temperature. Then the stoichiometric n-butyl titanate was add and stir for 20 min to make it evenly mixed to obtain a light yellow solution. Then stoichiometric dicyandiamide was dissolved in 150 mL of deionized water and mix with the above light yellow solution at 30 °C and stirred for 24 h. After aging for 2 days, freeze-dry was taken. The product was putted into an oven at 80 °C for 1 h, and then placed in a muffle furnace at 530 °C for 2 h.

Dicyandiamide as N source were added to the Ti gel. After calcination, TiO_2 nanoparticles with different nitrogen doping amounts were prepared, which were denoted as NT-1, NT-2, NT-3, and NT-4. The raw mole ratios of n-butyl titanate to dicyandiamide for NT-1, NT-2, NT-3 and NT-4 are 1.2, 0.6, 0.3, and 0.15 respectively.

SEM analysis was carried out using a field-emission scanning electron microscope Hitachi SU8010. TEM analysis was carried out by JEOL-2100F. The phase structure was detected by X-ray diffractometer Rigaku D/MAX-RB X-ray diffractometer. The diffractograms were recorded in a 2θ range between 10° and 80° in steps of 0.02 °. Raman spectroscopy was collected using the confocal Raman spectrometer Renishaw RM2000. The laser wavelength was 514 nm and the laser optical power was 0.5 mW. The IR spectrum was collected using the Perkin Elmer System 2000 infrared spectrometer. UV-vis spectrum in the region 250–800 nm was collected using Hitachi U-3010 ultraviolet-visible spectrophotometer.

The photocatalytic performance of the catalyst was evaluated by the liquid phase degradation of organic pollutants MB, rhodamine B (RhB), methylene orange (MO), phenol and dichlorophenol under ultraviolet light. The UV reaction used a 100 W (λ = 365 nm) mercury lamp. 25 mg of NT nanoparticle powder was put into 50 mL of organic pollutant ($C_0 = 2 \times 10^{-5}$ mol/L) solution. Then stirring for 1h made the probe molecules reach adsorption equilibrium on the surface of NT particles. When the light was turned on, the photocatalytic degradation reaction was carried. Samples of 2.5 mL were taken at different irradiation times and they were centrifuged (4000 rpm, 10 min) to separate NT particles. Then the supernatant was taken to detect the absorbance of colored organic pollutants (MB, RhB, MO) with a UV-vis spectrophotometer. High performance liquid chromatography was used to detect the electrical signals of DCP and phenol, and then the concentration changes of the target molecules in the solution were tracked.

The visible light catalytic activity of catalysts was evaluated by degrading MB molecules in water. A 500 W xenon lamp was used as the light source, and a filter (λ > 420 nm) was used to filter out ultraviolet light below 420 nm. Fifty mL of 3 $\times 10^{-5}$ mol/L MB solution was put into a quartz tube, and 25 mg of N-doped TiO_2 nanoparticles was added. Stirring for 20 min made MB molecules reach an adsorption equilibrium on the surface of N-doped TiO_2 particles. When the light was turned on, the photocatalytic degradation reaction was carried. Three mL of sample was taken at different irradiation times and centrifuged to separate the N-doped TiO_2 particles (4000 rpm, 10 min). The supernatant was taken and the absorbance was detected by a UV-vis spectrophotometer.

A 500 W xenon lamp was used as the light source, and a filter (λ > 420 nm) was used to filter out ultraviolet light below 420 nm. The electrochemical workstation CHI660B (Shanghai Chenhua Instrument Company) was used for the photoelectric performance test of the three-electrode system, which was achieved in a self-made three-electrode electrolytic cell with quartz window. The counter electrode is Pt wire; the reference electrode was a saturated calomel electrode; the working electrode was an N doped-TiO_2 membrane electrode; and the electrolyte was a 0.1 mol/L Na_2SO_4 solution. The scanning speed of the linear scanning measurement photocurrent is 50 mV/s.

3. Results and discussion

3.1. Characterization of catalysts

The crystal structures of TiO_2 with different nitrogen doping amounts prepared by sol-gel method were characterized by X-ray diffraction (XRD). As shown in Figure 1a, XRD spectra of all samples have similar spectral characteristics. It indicates that all samples crystallize as the single-phase anatase structure (JCPDS 21-1272) and the crystal shape of TiO_2 did not change after nitrogen doping. The peaks of N-doped TiO_2 show slightly shift to a smaller angle. It is speculated

that the doping nitrogen atom with large atomic radius replaces the oxygen atom in TiO_2, which makes the interplanar spacing in TiO_2 become larger. Raman spectroscopy is a sensitive technique to distinguish individual phase of TiO_2. Raman spectroscopy was exploited to further explore crystal properties of N-doped TiO_2. Figure 1b demonstrates the well-defined peaks located at 143 cm^{-1}, 396 cm^{-1}, 516 cm^{-1}, and 638 cm^{-1} can be respectively assigned the vibrational modes of E_g, B_{1g}, $B_{1g} + A_{1g}$ and E_g of the anatase phase. No other obvious new peaks appear in the Raman spectrum after doping N, indicating the nanoparticles contain exclusively anatase [33].

Revealed in the SEM images (Figure 2) and TEM image (Figure S1), the N-doped TiO_2 particles look spherical, with similar nanoparticle sizes of about 15 nm and good dispersity. Figure 3a shows the UV-visible absorption spectrum of the samples. It can be seen that the absorption of N-doped TiO_2 is generally stronger than that of TiO_2. Particularly, the N doping causes stronger absorption capacity in the visible light region, and we can see the red shift of the absorption edge, which indicates that the band gap of TiO_2 is narrowed. The bandgaps calculated from the Tauc plots of bare TiO_2, NT-1, NT-2, NT-3, NT-4 are 3.22eV, 3.19 eV, 3.13 eV, 3.06 eV, 3.20 eV. It can be deduced that the 2p states of the doped nitrogen atoms mixing with O 2p states contributed to the band gap narrowing. Due to the narrower band gap, an electron could be excited easily from the valence band to the conduction band in the N-doped TiO_2, which is helpful in increasing the photocatalytic activity. In other side, the absorption (bandgap) increases (decreases) as N-doping increases from NT-1 to NT-3. However, in the NT-4, the absorption (bandgap) decreases (increases) again, which suggests that proper amount of doping is important. The X-ray photoelectron spectroscopy (XPS) was carried out to scan the binding energy range of N 1s (Figure S2). It exhibits the binding energy of N 1s at 397 eV, originating from Ti-N bonds in TiO_2 lattice [23,34], whereas the peak at 400 eV was consistent with the adsorbed nitrogen N_2 on the surface of TiO_2 [23].

Figure 3b shows the infrared spectra of the samples. The wide absorption peak at 3230 cm^{-1} is caused by the stretching vibration of O-H. The absorption peak at 1643 cm^{-1} is caused by the bending vibration of O-H. The above two peaks exist both in TiO_2 and N-doped TiO_2, and the peak in N-doped TiO_2 is strengthened. It needs to be noted that there are several new peaks in N-doped TiO_2, located at 3624, 3728 cm^{-1}, 2289 cm^{-1}, 1330 cm^{-1} and 700 cm^{-1}. The peaks at 3624, 3728 cm^{-1} and 2289 cm^{-1} correspond to the N-containing groups adsorbed on the surface of TiO_2 nanoparticles, i.e. –NH_2 and –CN in dicyandiamide. The peak at 1330cm^{-1} is presumed to be the characteristic absorption peak of Ti-OH. The characteristic absorption peak at 700 cm^{-1} is derived from the N-Ti-O structure formed by N atoms replacing O atoms in the TiO_2, which indicates that N atoms not only exist in the gaps of TiO_2 lattice, but also replace part of the O atoms in the TiO_2 lattice.

3.2. Photocatalytic activity

The photocatalytic activity of the samples was measured in terms of the relative concentration of target pollutants. The colored target pollutants have typical absorbance peaks, and consequently their concentrations can be readily determined
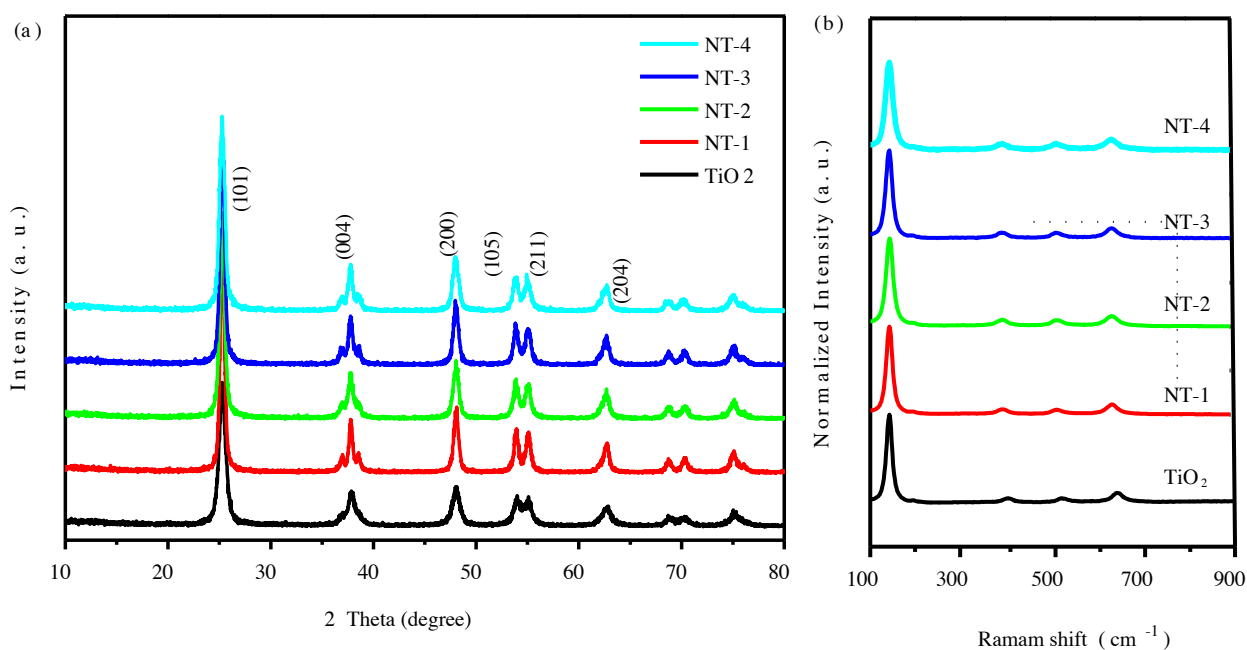

Figure 1. XRD patterns (a) and Raman spectra (b) of the anatase N-doped TiO_2 nanoparticles.
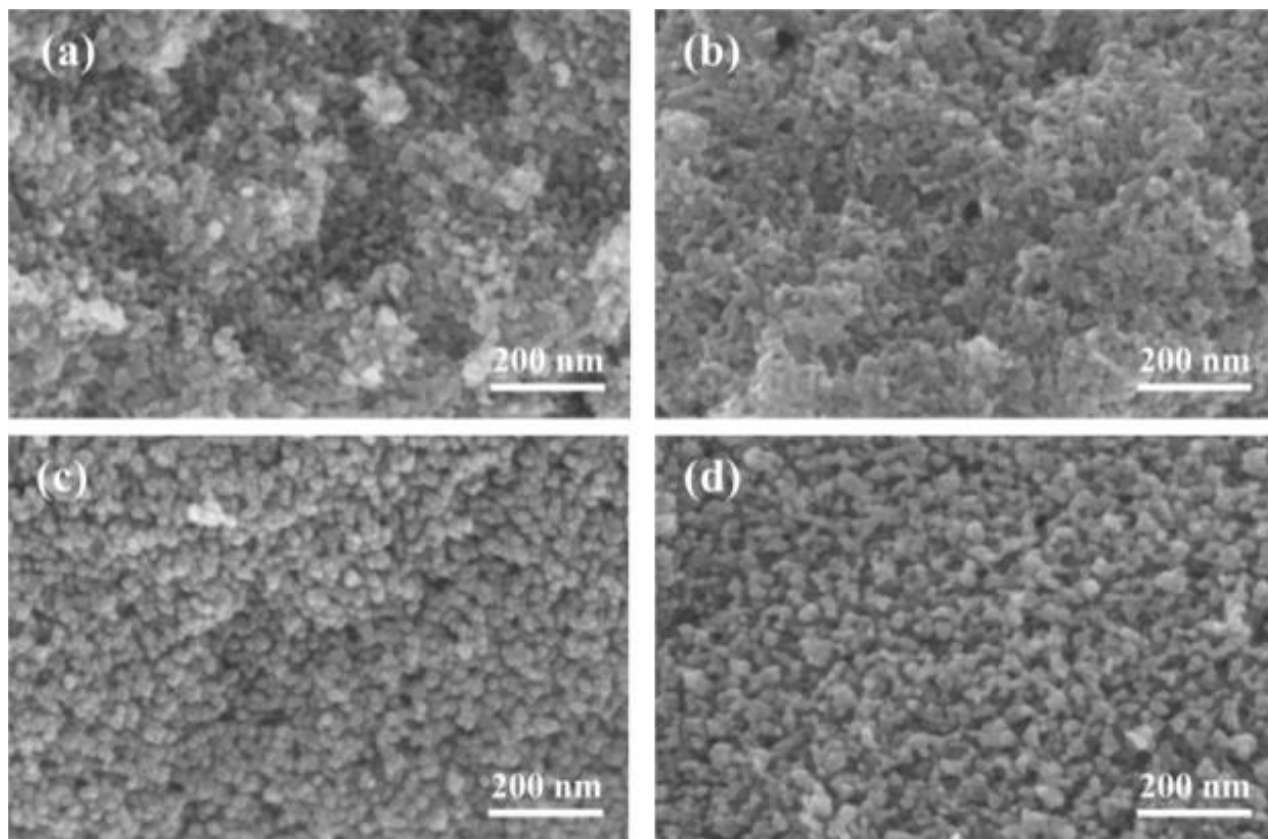
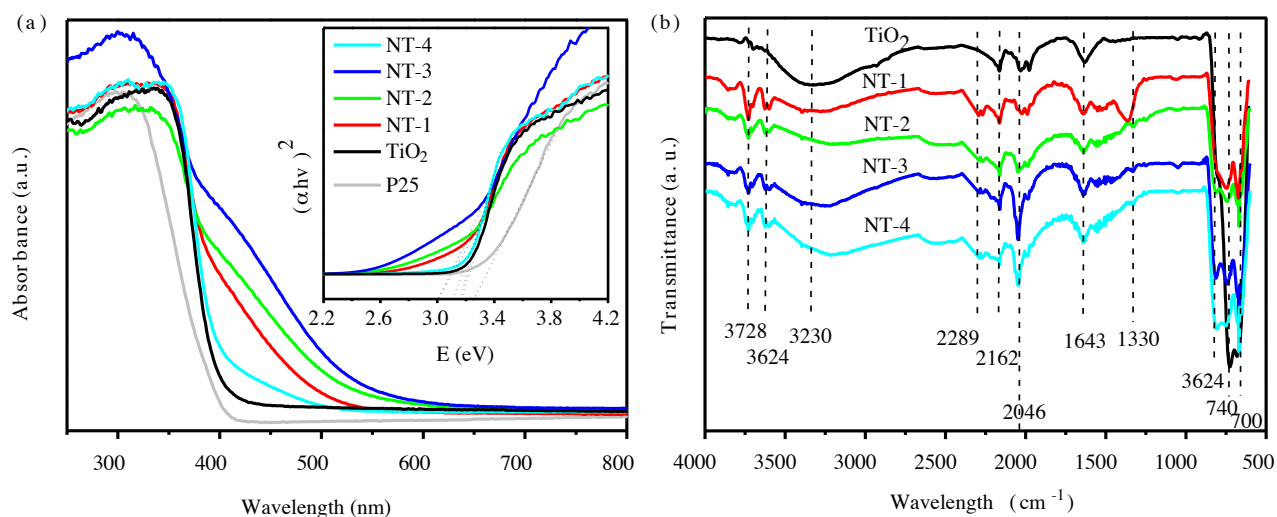**Figure 2.** SEM image of the anatase N-doped TiO$_2$ nanoparticles of NT-1(a), NT-2(b), NT-3(c) and NT-4(d).

Figure 3. UV-vis absorbtion spectra (a) and infrared spectra (b) of N-doped TiO$_2$.

by a UV–vis spectrophotometer. Firstly, with 2×10^{-5} mol/L MB as the target pollutant, the degradation ability of the N-doped TiO$_2$ catalyst under ultraviolet light was tested, as shown in Figure 4. It is found that all the N-doped TiO$_2$ photocatalysts display superior photocatalytic behaviors to the bare TiO$_2$. The activity of N-doped TiO$_2$ gradually increases as the doping concentration going up, then tends to drops, which suggests that excessive N will depress the activity. NT-3 present the far greater degradation activity than that of other samples of the same series prepared by the sol-gel method, and even comparable to the performance of P25 prepared by the flame method from the commercial company. It produced
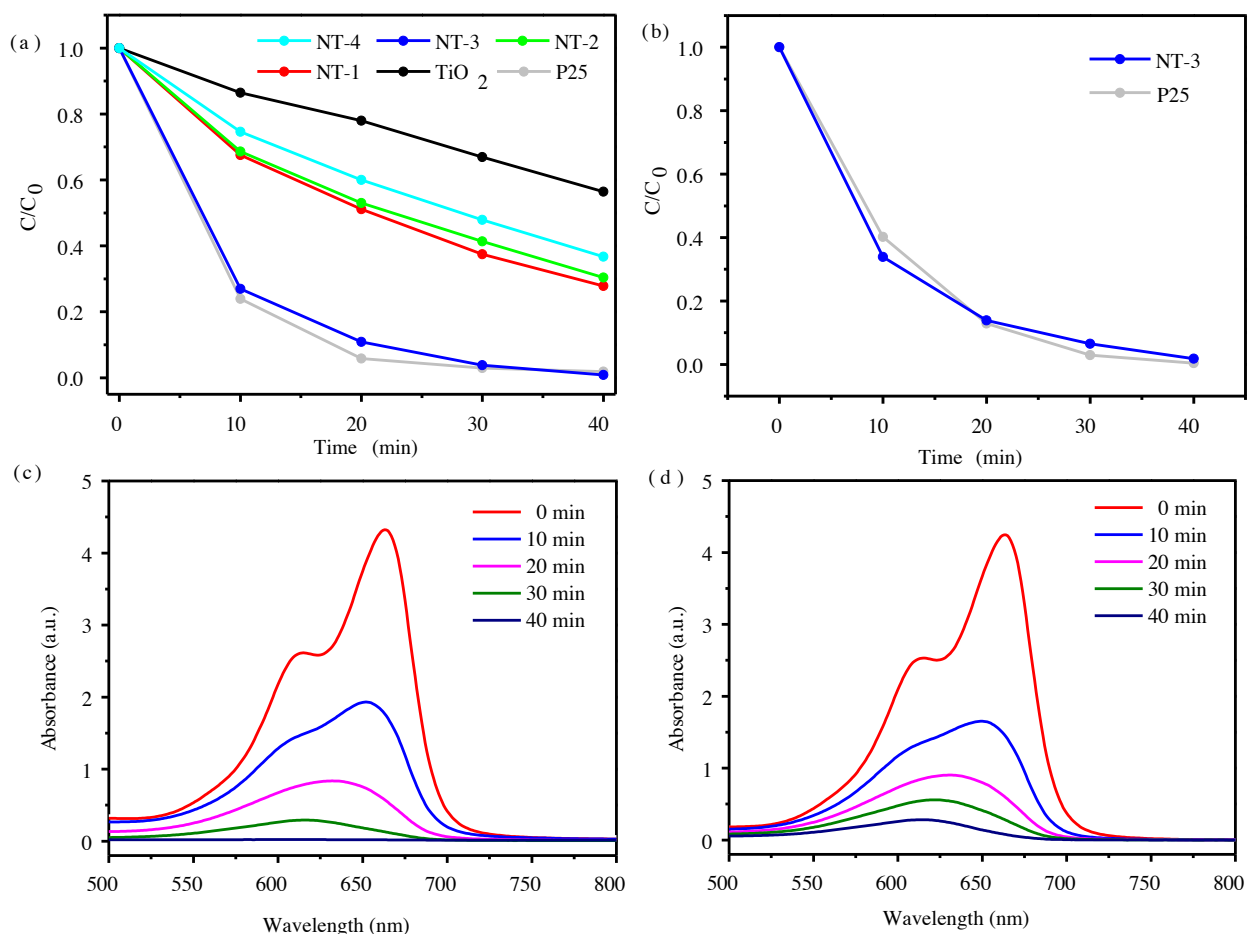
Figure 4. (a) Photocatalytic degradation of 2×10^{-5} mol/L MB aqueous solution by N-doped TiO_2 and P25. (b) Photocatalytic degradation of 3×10^{-5} mol/L MB aqueous solution by NT-3 and P25. UV-vis absorption spectrum of MB aqueous solution with N-doped TiO_2 (c) and P25 (d) photocatalysts at different degradation time; the initial concentration of MB is 3×10^{-5} mol/L.

approximately 100% conversion of MB within 40 min (Figure 4a). In order to further study the ultraviolet activity of NT-3 and P25, we then increased the MB concentration to 3×10^{-5} mol/L. Figure 4b shows the evolution of MB concentration at each time interval, which are derived from the absorption spectra (Figures 4c & 4d). It can be seen that NT-3 and P25 degrade MB simultaneously. The time it takes for NT-3 to completely degrade MB is almost the same as that of P25.

The ultraviolet activity of N-doped TiO_2 to other target molecules are also tested and show different results. For organic color dyes, Figure 5a shows the degradation of RhB under UV light. NT-3 takes 3 times as much time to degrade RhB completely as P25. Figure 5b shows the degradation of MO under UV light. After 30 min of light reaction, neither of NT-3 and P25 can completely degrade it, and the degradation ability of NT-3 is also worse than that of P25. MB and RhB are cationic dyes, while MO is an anionic dye. The results show that NT-3 is more capable of degrading cationic dyes than anionic dyes. In order to explain the selectivity of degrading organic color dyes, a series of samples were tested for Zeta potential, as shown in Table. The NT-3 is the most negative, indicating that it has a strong negative charge and is easy to attract cations. It is speculated that after the cationic dyes on the surface of NT-3 are degraded under ultraviolet light, the surrounding dye ions can be quickly supplemented to the catalyst surface because of the electrostatic attraction, thus accelerating the degradation rate and show the selectivity.

For organic colorless pollutants, almost complete degradation is achievable. While, NT-3 takes 4 times as much time to degrade dichlorophen (DCP) completely as P25 (Figure 5c) and takes 3 times as much time to degrade phenol completely as P25 (Figure 5d). As can be seen, the degradation ability of NT-3 is reduced for these colorless small-molecular organics compared with the degradation of MB.

Taking MB as the target pollutant, the degradation ability of the catalysts under visible light was also tested, as shown in Figure 6a. NT-3 has the strongest degradation activity, which is consistent with the strongest degradation activity
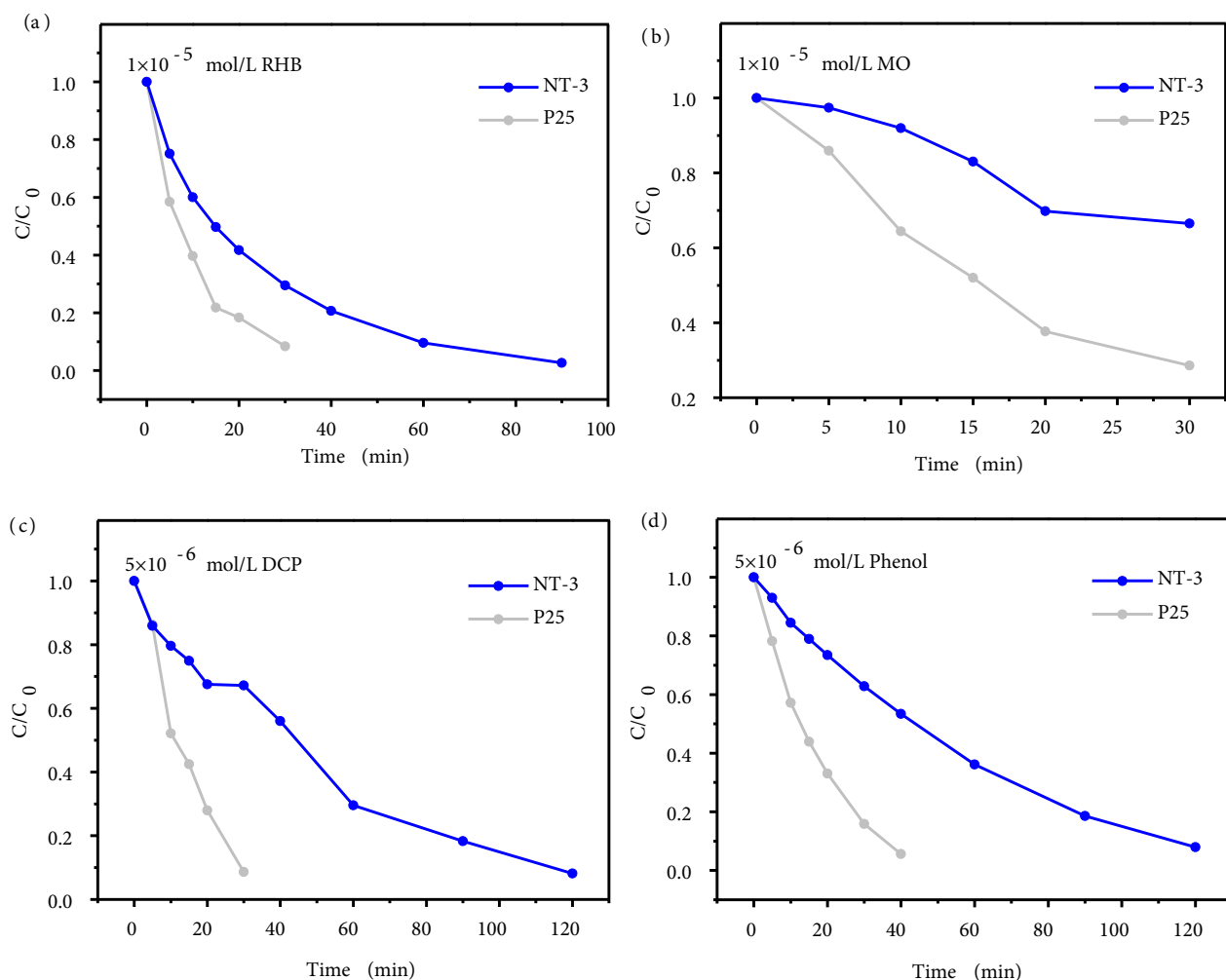
Figure 5. Photocatalytic degradation of RHB (1×10^{-5} mol/L) (a), MO (1×10^{-5} mol/L) (b), DCP (5×10^{-6} mol/L) (c), phenol (5×10^{-6} mol/L) (d) aqueous solution by N-doped TiO_2 and P25.

Table. Zeta potential of N-doped TiO_2 and P25.

Sample	NT-1	NT-2	NT-3	NT-4	TiO_2	P25
Zeta potential (mV)	−64.7	−53.8	−71.7	−55.1	−9.2	−10.1

under ultraviolet light, indicating that the negatively charged nature of the material is also conducive to the adsorption-degradation under visible light. The good photocatalytic activity of NT-3 is related to the efficient absorption of light and the separation of photogenerated electrons and holes. We further analyze it through the photocurrent test. Figure 6b shows the photocurrent of N-doped TiO_2 photocatalysts under visible light. It indicates that the photoresponse current of the NT-3 sample is the strongest, which is consistent with the best photocatalytic activity of NT-3 in the N-doped TiO_2.

Phenol is a typical organic pollutant with high resistance to direct photolysis and oxidation under visible light. Therefore, we also use phenol as a degradation object under visible light. As shown in Figure S3, phenol can be degraded to a certain extent by N-doped TiO_2, bare TiO_2 or P25. Although the appropriate amount of N doping can make the photocatalytic performance much better than bare TiO_2 or P25, N-doped TiO_2 can only degrades ~10% of the phenol in seven hours. Compared with the above organic pollutants, the degradation efficiency of phenol is low. To achieve efficient degradation of phenol under visible light, it may be necessary to further modify the photocatalyst or combine with other catalytic methods.
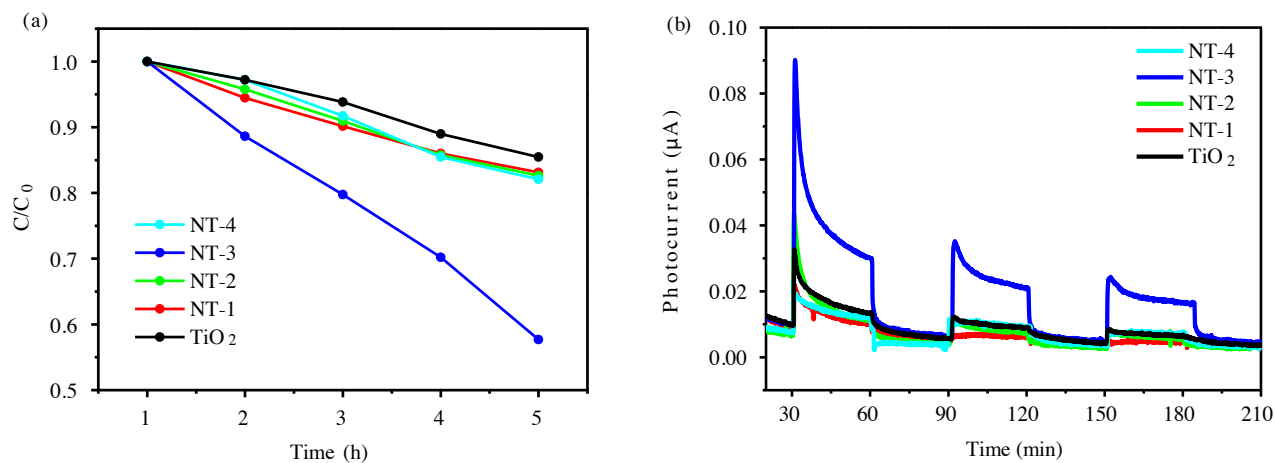
Figure 6. (a) Photocatalytic degradation of 3×10^{-5} mol/L MB aqueous solution by N-doped TiO$_2$ under visible light. (b) Photocurrent of N-doped TiO$_2$.

4. Conclusion

N-doped TiO$_2$ was favorably synthesized by a simple sol-gel method, with dicyandiamide used as N source. Doping N into TiO$_2$ boosts the light response capacity and promotes the generation of carriers, consequently ameliorating the catalytic activity, especially visible light responsive photocatalytic activity. The doping ratio possesses a considerable effect on the activity of TiO$_2$. The resulting TiO$_2$ doped with an appropriate amount of N exhibits high photocatalytic activity for the degradation of MB under ultraviolet and visible light, which is attributed to the appropriate dispersibility and crystallinity, modified zeta potential and enhanced absorption. This work provides a feasible route for improving the visible photocatalytic activity of nonmetal-ion-doped TiO$_2$, which show the potential application to other oxides with wide bandgap energies.

Acknowledgment

References

1. Zhang P, Tachikawa T, Fujitsuka M, Majima T. In situ fluorine doping of TiO$_2$ superstructures for efficient visible-light driven hydrogen generation. ChemSusChem 2016; 9: 617-623. doi: 10.1002/cssc.201501558

2. Abdelhaleem A, Chu W, Liang XL. Diphenamid degradation via sulfite activation under visible LED using Fe (III) impregnated N-doped TiO$_2$ photocatalyst. Applied Catalysis B: Environmental 2019; 244: 823-835. doi: 10.1016/j.apcatb.2018.11.085

3. Yang YQ, Yin LC, Gong Y, Niu P, Wang JQ et al. An unusual strong visible-light absorption band in red anatase TiO$_2$ photocatalyst induced by atomic hydrogen-occupied oxygen vacancies. Advanced Materials 2018; 30: 1704479. doi: 10.1002/adma.201704479

4. Lian ZC, Wang WC, Li GS, Tian FH., Schanze KS et al. Pt-enhanced mesoporous Ti^{3+}/TiO$_2$ with rapid bulk to surface electron transfer for photocatalytic hydrogen evolution. ACS Applied Materials & Interfaces 2017; 9: 16959-16966. doi: 10.1021/acsami.6b11494

5. Katal R, Salehi M, Farahano MHDA, Masudy-Panah S, Ong SL et al. Preparation of a new type of black TiO$_2$ under a vacuum atmosphere for sunlight photocatalysis. ACS Applied Materials & Interfaces 2018; 10: 35316-35326. doi: 10.1021/acsami.8b14680

6. He RZQ, Xu X, Song S, Xie L, Tu JJ et al. A visible light-driven titanium dioxide photocatalyst codoped with lanthanum and iodine: an application in the degradation of oxalic acid. The Journal of Physical Chemistry C 2008; 112: 16431. doi: 10.1021/jp803291c

7. Asahi R, Morikawa T, Ohwaki K, Taga Y. Visible-light photocatalysis in nitrogen-doped titanium oxides. Science 2001; 293: 269-271. doi: 10.1126/science.1061051

8. Xu C, Killmeyer R, Gray LM, Khan SUM. Photocatalytic effect of carbon-modified n-TiO$_2$ nanoparticles under visible light illumination. Applied Catalysis B: Environmental 2006; 64: 312-317. doi: 10.1016/j.apcatb.2005.11.008

9. Dvoranova D, Brezova V, Mazur M, Malati MA. Investigations of metal-doped titanium dioxide photocatalysts. Applied Catalysis B: Environmental 2002; 37 (2): 91–105. doi: 10.1016/S0926-3373(01)00335-6

10. Jagadale TC, Takale SP, Sonawane RS, Joshi HM, Patil SI et al. N-doped TiO$_2$ nanoparticle based visible light photocatalyst by modified peroxide sol−gel method. The Journal of Physical Chemistry C 2008; 112: 14595. doi: 10.1021/jp803567f

11. Zhang Z, Long J, Xie X, Zhuang H, Zhou Y et al. Controlling the synergistic effect of oxygen vacancies and N dopants to enhance photocatalytic activity of N-doped TiO$_2$ by H$_2$ reduction. Applied Catalysis A: General 2012; 425-426: 117-124. doi: 10.1016/j.apcata.2012.03.008

12. Zhang YC, Yang M, Zhang G, Dionysiou DD. HNO$_3$-involved one-step low temperature solvothermal synthesis of N-doped TiO$_2$ nanocrystals for efficient photocatalytic reduction of Cr(VI) in water. Applied Catalysis B: Environmental 2013; 142-143: 249-258. doi: 10.1016/j.apcatb.2013.05.023

13. Zhang G, Zhang YC, Nadagouda M, Han C, O'Shea K et al. Visible light-sensitized S, N and C co-doped polymorphic TiO$_2$ for photocatalytic destruction of microcystin-LR. Applied Catalysis B: Environmental 2014; 144: 614-621. doi: 10.1016/j.apcatb.2013.07.058

14. Huang J, Dou L, Li J, Zhong J, Li M, Wang T. Excellent visible light responsive photocatalytic behavior of N-doped TiO$_2$ toward decontamination of organic pollutants. Journal of Hazardous Materials 2021; 403: 123857. doi: 10.1016/j.jhazmat.2020.123857

15. Xie M, Feng Y, Luan Y, Fu X, Jing L. Facile synthesis of N-doped TiO$_2$ and its enhanced photocatalytic activity for degrading colorless pollutants. ChemPlusChem 2014; 79: 737-742. doi: 10.1002/cplu.201400021

16. Wang Z, Cai W, Hong X, Zhao X, Xu F et al. Photocatalytic degradation of phenol in aqueous nitrogen-doped TiO$_2$ suspensions with various light sources. Applied Catalysis B: Environmental 2005; 57: 223-231. doi: 10.1016/j.apcatb.2004.11.008

17. Feng XY, Wang PF, Hou J, Qian J, Ao YH. Significantly enhanced visible light photocatalytic efficiency of phosphorus doped TiO$_2$ with surface oxygen vacancies for ciprofloxacin degradation: Synergistic effect and intermediates analysis. Journal of Hazardous Materials 2018; 351: 196-205. doi: 10.1016/j.jhazmat.2018.03.013

18. Wang Y, Feng CX, Zhang M, Yang JJ, Zhang Z. Enhanced visible light photocatalytic activity of N-doped TiO$_2$ in relation to single-electron-trapped oxygen vacancy and doped-nitrogen. Applied Catalysis B: Environmental 2010; 100: 84-90. doi: 10.1016/j.apcatb.2010.07.015

19. Drozd VS, Zybina NA, Abramova KE, Parfenov MY, Kumar U et al. Oxygen vacancies in nano-sized TiO$_2$ anatase nanoparticles. Solid State Ionics 2019; 339: 115009-115016. doi: 10.1016/j.ssi.2019.115009

20. Qi W, Zhang F, An XQ, Liu HJ, Qu JH. Oxygen vacancy modulation of {010}-dominated TiO$_2$ for enhanced photodegradation of sulfamethoxazole. Catalysis Communications 2019; 118: 35-38. doi: 10.1016/j.catcom.2018.09.014

21. Zhao B, Wang X, Zhang YZ, Gao JN, Chen ZW et al. Synergism of oxygen vacancies, Ti^{3+} and N dopants on the visible-light photocatalytic activity of N-doped TiO$_2$. Journal of Photochemistry and Photobiology A: Chemistry 2019; 382: 111928-111934.

22. Xu L, Ma X, Sun N, Chen F. Bulk oxygen vacancies enriched TiO$_2$ and its enhanced visible photocatalytic performance. Applied Surface Science 2018; 441: 150-155. doi: 10.1016/j.apsusc.2018.01.308

23. Hao L, Miyazawa K, Yoshida H, Lu Y. Visible-light-driven oxygen vacancies and Ti^{3+} co-doped TiO$_2$ coatings prepared by mechanical coating and carbon reduction. Materials Research Bulletin 2018; 97: 13-18. doi: 10.1016/j.materresbull.2017.08.023

24. Irie H, Watanabe Y, Hashimoto K. Nitrogen-concentration dependence on photocatalytic activity of TiO$_{2-x}$N$_x$ powders. The Journal of Physical Chemistry B 2003; 107: 5483-5486. doi: 10.1021/jp030133h

25. Torres GR, Lindgren T, Lu J, Granqvist C, Lindquist S. Photoelectrochemical study of nitrogen-doped titanium dioxide for water oxidation. The Journal of Physical Chemistry B 2004; 108: 5995-6003. doi: 10.1021/jp037477s

26. Nakamura R, Tanaka T, Nakato Y. Mechanism for visible light responses in anodic photocurrents at N-doped TiO$_2$ film electrodes. The Journal of Physical Chemistry B 2004; 108: 10617-10620. doi: 10.1021/jp048112q

27. Kobayakawa K, Murakami Y, Sato Y. Visible-light active N-doped TiO$_2$ prepared by heating of titanium hydroxide and urea. Journal of Photochemistry and Photobiology A: Chemistry 2005; 170: 177-179. doi: 10.1016/j.jphotochem.2004.07.010

28. D'Arienzo M, Scotti R, Wahba L, Battocchio C, Bemporad E et al. Hydrothermal N-doped TiO$_2$: Explaining photocatalytic properties by electronic and magnetic identification of N active sites. Applied Catalysis B: Environmental 2009; 93: 149-155. doi: 10.1016/j.apcatb.2009.09.024

29. Wang YQ, Yu XJ, Sun DZJ. Synthesis, characterization, and photocatalytic activity of TiO$_{2-x}$N$_x$ nanocatalyst. Journal of Hazardous Materials 2007; 144: 328-333. doi: 10.1016/j.jhazmat.2006.10.033

30. Mrowetz M, Balcerski W, Colussi AJ, Hoffmann MR. Oxidative power of nitrogen-doped TiO$_2$ photocatalysts under visible illumination. The Journal of Physical Chemistry B 2012; 108: 17269-17273. doi: 10.1021/jp0467090

31. Nolan NT, Synnott DW, Seery MK, Hinder SJ, Wassenhoven AV et al. Effect of N-doping on the photocatalytic activity of sol–gel TiO$_2$. Journal of Hazardous Materials 2012; 211: 88-94. doi: 10.1016/j.jhazmat.2011.08.074

32. Qian NX, Zhang X, Wang M, Sun X, Sun XY et al. Great enhancement in photocatalytic performance of (001)-TiO$_2$ through N-doping via the vapor-thermal method. Journal of Photochemistry and Photobiology A: Chemistry 2020; 386: 112127. doi: 10.1016/j.jphotochem.2019.112127

33. Sutiono H, Tripathi AM, Chen HM, Chen CH, Su WN et al. Facile synthesis of [101]-oriented rutile TiO$_2$ nanorod array on FTO substrate with a tunable anatase-rutile heterojunction for efficient solar water splitting. ACS Sustainable Chemistry & Engineering 2016; 4: 5963-5971. doi: 10.1021/acssuschemeng.6b01066

34. Aita Y, Komatsu M, Yin S, Sato T. Phase-compositional control and visible light photocatalytic activity of nitrogen-doped titania via solvothermal process. Journal of Solid State Chemistry 2004; 177: 3235-3238. doi: 10.1016/j.jssc.2004.04.048
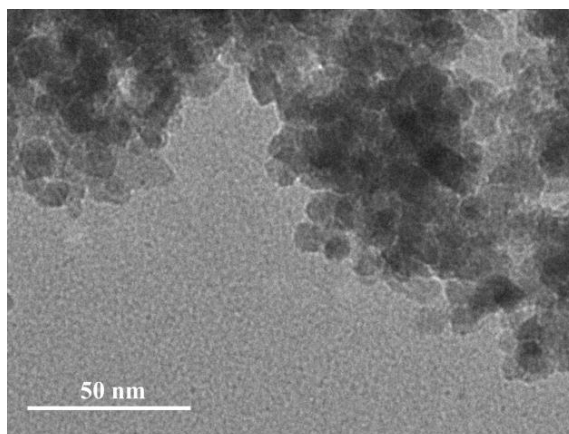
Supplementary data
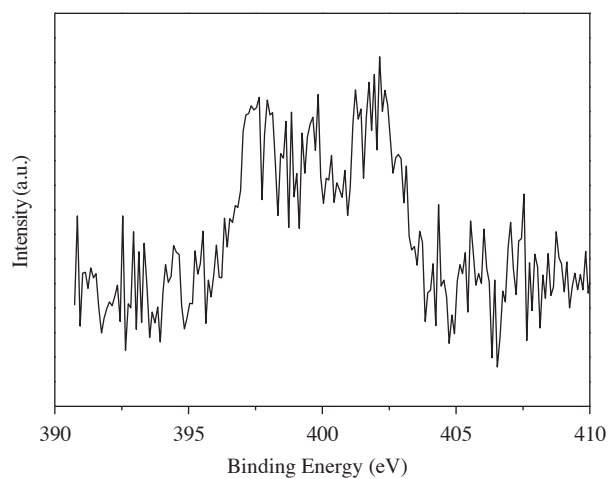

Figure S1. TEM image of NT-3.
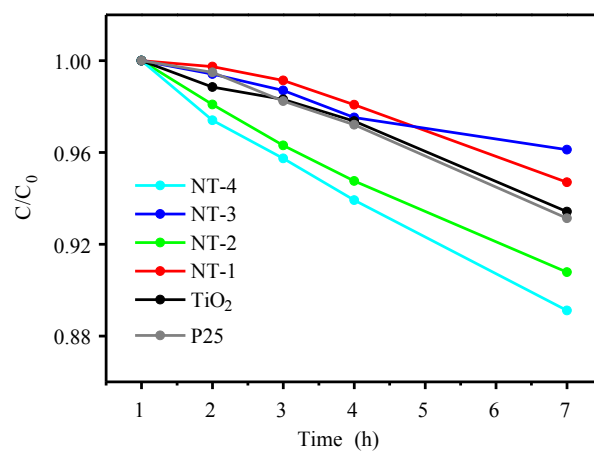

Figure S2. XPS spectra of N-doped TiO_2.

Figure S3. Photocatalytic degradation of 5×10^{-6} mol/L phenol aqueous solution by N-doped TiO_2 under visible light.